

Effect of Architecture and Porosity on Mechanical Properties of Borate Glass Scaffolds Made by Selective Laser Sintering

Krishna C. R. Kolan¹, Ming C. Leu¹, Gregory E. Hilmas² and Taylor Comte^{1,3}

¹Department of Mechanical and Aerospace Engineering, Missouri University of Science and Technology, Rolla, MO 65409

²Department of Materials Science and Engineering, Missouri University of Science and Technology, Rolla, MO 65409

³Department of Biomedical Engineering, University of North Carolina, Chapel Hill, NC 27514

Abstract

The porosity and architecture of bone scaffolds, intended for use in bone repair or replacement, are two of the most important parameters in the field of bone tissue engineering. The two parameters not only affect the mechanical properties of the scaffolds but also aid in determining the amount of bone regeneration after implantation. Scaffolds with five different architectures and four porosity levels were fabricated using borate bioactive glass (13-93B3) using the selective laser sintering (SLS) process. The pore size of the scaffolds varied from 400 to 1300 μm . The compressive strength of the scaffolds varied from 1.7 to 15.5 MPa for porosities ranging from 60 to 30%, respectively, for the different architectures. Scaffolds were soaked in a simulated body fluid (SBF) for one week to measure the variation in mechanical properties. The formation of the Hydroxyapatite and *in-vitro* results are provided and discussed.

1. Introduction

The discovery of Bioglass[®] by Prof. Hench in 1969 has led to active research interest in the field of bioactive materials in the past four decades [1, 2]. The bioactive materials convert to Hydroxyapatite (HA), the main mineral constituent of bone, when exposed to body fluids thereby integrating with the surrounding tissue. Recently, interest has been focused on developing bioactive glasses as they offer excellent bioactive characteristics when compared to glass-ceramics or ceramics. Borate based bioactive glasses not only bond to the surrounding hard tissue but are also known to bond with soft tissues [3]. Table 1 shows the compositions (in wt.%) of the borate based 13-93B3 bioactive glass when compared to the silicate based 13-93 bioactive glass. The 45S5 glass composition is also presented for comparison. The molar concentration of SiO_2 in 13-93 glass is replaced by B_2O_3 in the 13-93B3 glass. Borate glass is chemically less durable when compared to the silicate glass and therefore, it converts to HA at a faster rate and allows faster bone formation when compared to the silicate glass [3, 4].

Table 1. Compositions (in wt.%) of 13-93 and 13-93B3 glasses compared to 45S5 glass.

	SiO_2	P_2O_5	CaO	MgO	Na_2O	K_2O	B_2O_3
45S5	45	6	24.5	-	24.5	-	-
13-93	53	4	20	5	6	12	-
13-93B3	-	3.7	18.5	4.6	5.5	11.1	56.6

Recently, 13-93B3 glass scaffolds, with ~50% porosity, were fabricated with an organic based paste composition using the Robocasting technique [5, 6]. Organic solvents were used in

the above studies to prepare the paste because of the reactivity of borate glass with aqueous based solvents. Although porosity and pore size can be controlled using Robocasting, the process has limited control over the pore architecture when fabricating porous parts because of the layer-by-layer filament deposition. In comparison, powder based additive manufacturing (AM) techniques like the selective laser sintering (SLS) process provide flexibility in fabricating scaffolds with complex pore architectures as they do not require support structures during part fabrication. Therefore, the SLS process provides an opportunity to investigate the effects of porosity and pore architecture on the structural and biological characteristics of the scaffolds. There have been some articles in the literature wherein researchers have proposed techniques to develop the CAD models for scaffolds which closely mimic the human trabecular bone architecture [7-9]. However, fabricating scaffolds with such a complex architecture is still a challenge as not all AM techniques can fabricate them with bioceramics at the required resolution [10]. Also, limited work has been done to compare the bioactive scaffolds made with complex architectures and the traditional lattice structures, considering the aspects of both manufacturability and their behavior after *in vitro* or *in vivo* tests. In our previous work, we have shown that silicate based 13-93 bioactive glass scaffolds made by the SLS process provide good mechanical properties and preferable surface morphology for cell proliferation [11-13]. A low laser power and energy density was employed during the fabrication, resulting only melting the polymeric binder and assisting in fusion of the bioactive glass particles without affecting the material properties of the borate glass. Here, we hypothesized that scaffolds can be fabricated with 13-93B3 bioactive glass using the same processing parameters as established in our previous work [13].

In the current work, we investigated the effects of pore architecture and porosity on the mechanical properties of the scaffolds. Five different architectures were considered and the scaffolds were fabricated with each of these architectures at four designed porosity levels. The sintered scaffolds were immersed in simulated body fluid (SBF) for one week and the effects of architecture and porosity on the compressive resistance of the scaffolds were studied. The materials and methods used for this study are noted in Section 2. The results obtained, including the variation of compressive strength with respect to porosity and architecture, before and after immersion in SBF, are presented in Section 3.

2. Materials and Methods

2.1. Fabrication of scaffolds

13-93B3 bioactive glass (prepared by Mo-Sci Corp., Rolla, MO) with a nominal chemical composition of 56.6% B₂O₃, 3.7% P₂O₅, 18.5% CaO, 4.6% MgO, 5.5% Na₂O and 11.1% K₂O (by weight) was used in this research. The average particle size of the 13-93B3 particles was measured to be ~12 μm (d₅₀), with a d₁₀ of 4 μm and a d₉₀ of 30 μm. Particle size distributions were obtained using a laser diffraction-based particle size analyzer (S3500, Microtrac Inc., Largo, FL). The 13-93B3 glass particles were mixed with stearic acid as the binder (C₁₈H₃₆O₂, grade HS, Acros Organics, Morris Plains, NJ) and dry ball-milled for 8 hrs with ZrO₂ milling media to obtain the feedstock powder for the SLS machine. A 15% binder content by weight was used for this purpose as this quantity provides the best possible results and is based on our previous study of SLS using 1393 bioactive glass [13]. The fabrication experiments were carried out on a commercial DTM Sinterstation 2000 machine. The effect of SLS parameters on

fabricating scaffolds using stearic acid binder and bioglass powders has already been investigated in our previous work and the same set of parameters (laser power – 5 W, scan speed – 508 mm/s, scan spacing – 0.23 mm, layer thickness – 76.2 μm) were adopted for the current study [13].

2.2. Post-processing and physical assessment of scaffolds

The fabricated green parts were post-processed in a three-stage programmable air furnace (Vulcan Benchtop Furnace, York, PA). The following heat treatment schedule was used for this study: de-binding heating rate of 0.1°C/min to 550°C; increase in the heating rate to 1°C/min until a final sintering temperature of 570°C with a 1 hour hold; and then the furnace was turned off and allowed to cool to room temperature. Optical microscopy was used to measure the pore sizes of the sintered scaffolds. Archimedes method was used to measure the apparent porosity of the sintered scaffolds. Cubic shaped parts measuring 1 cm in length were used for the purpose of measuring porosity and parts measuring 5 mm in length were used for the purpose of mechanical testing and SBF study. A cross-head speed of 0.5 mm/min was used on a mechanical load frame (Instron 4469 UTM, Norwood, MA) to determine the compressive strengths of the parts. Five samples in each set were used, and the results were reported as the average value \pm the standard deviation. Scans were run from 2θ values ranging from 10° to 80° using Cu K α radiation ($\lambda = 0.154056$ nm) for powder X-ray diffraction (XRD) analysis (Philips X-Pert, Westborough, MA) on the as-received 13-93B3 powder, sintered scaffolds and also on the dried scaffolds after removing them from the SBF to determine the changes in the crystalline/amorphous nature of the material.

2.3. SBF tests

The SBF solution was prepared based on the Kokubo method [14]. All the samples were ultrasonically cleaned three times using ethanol and then dried in an oven overnight before being kept in the SBF solution. The scaffolds were weighed and 100 ml of solution was used for 1 gram of the scaffold for soaking. The SBF solution container with scaffolds was kept in an incubator maintained at 37°C. All the compression tests were conducted on wet scaffolds to provide realistic data on the degradation of the scaffolds. Three samples in each set were used for compression testing and the results are reported as the average value \pm the standard deviation. The scanning electron microscopy (SEM) (S-570, Hitachi Co., Tokyo, Japan) images were obtained to analyze the surface morphology of the scaffolds.

3. Results and Discussion

3.1. Fabrication of Scaffolds

The CAD models of the repeatable units of the five architectures considered in this work are shown in Figure 1(a). The first unit cube is modeled by the solid tubular structures which are perpendicular to each other and running in x, y, and z directions. The porosity in this “cubic” architecture is a function of the diameter of the tube and distance between the tubes. The second unit cube is formed by subtracting a sphere from a solid cube and is termed as “spherical” pore architecture based on the geometry of the pore formed because of the design. The porosity in this

case is a function of the diameter of the sphere and length of the unit cube. The third unit cube is formed by diagonally joining the corners of a unit cube with tubular structures and is termed the “X” architecture. The porosity of the “X” architecture is a function of diameter of the tubes. The latter three architectures are the typical and frequently used designs in most of the AM techniques to manufacture scaffolds. The fourth and fifth are “diamond” and “gyroid” architectures, which are based on the freeform surface and try to mimic the trabecular architecture of bone. The surface was generated using open source software K3DSurf v0.6.2 [15]. The governing mathematical equations of these architectures can be modified to establish a range of porosities. The equation for gyroid surface is represented as:

$$\cos x \sin y + \cos y \sin z + \cos z \sin x - k = 0, \text{ where, } 0 \leq k \leq 1 \text{ and } -\pi \leq x, y, z \leq \pi;$$

and for a diamond surface, the governing equation is represented as:

$$\sin x \sin y \sin z + \sin x \cos y \cos z + \cos x \sin y \cos z + \cos x \cos y \sin z - k = 0, \text{ where, } 0 \leq k \leq 1 \text{ and } 0 \leq x, y, z \leq \pi;$$

The surface generated was modeled into a volume with the help of pre-processor software and then converted to a .STL file for fabrication using the SLS machine. The aspect of manufacturability was considered during the design process for all the scaffolds. For example, in the spherical architecture, a reduction in porosity was achieved by decreasing the diameter of the sphere to be subtracted from the cube. However, decreasing the diameter of the sphere will decrease the pore diameter and removing unsintered powder from fine pores after fabrication becomes limited, increasing the likelihood of damaging the scaffold structure. Therefore, the pore sizes of all the scaffolds were designed in such a way that the unsintered powder could be removed after the scaffold fabrication. The fabricated scaffolds after binder burnout and sintering are shown in Figure 1(b) as representative specimens from each of the architectures in the same order as shown in Figure 1(a).

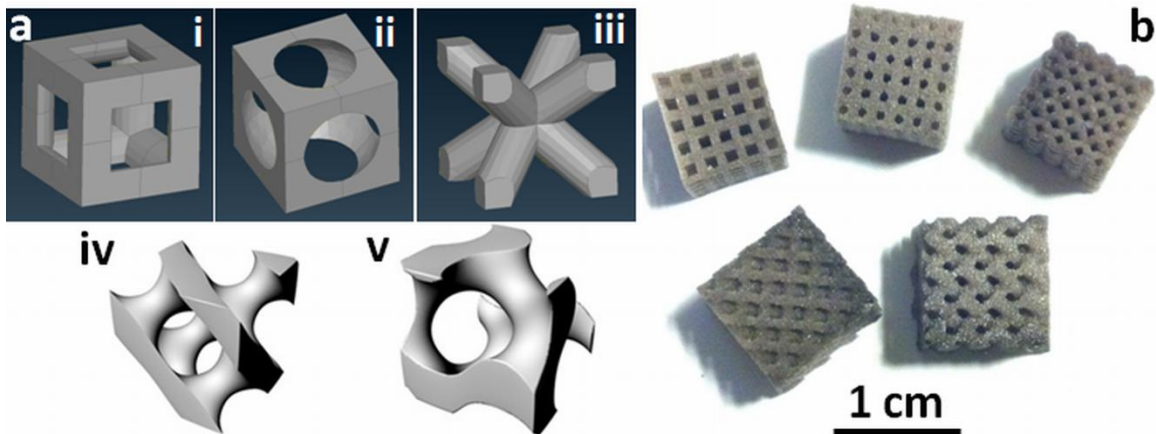


Figure 1. (a) CAD models of the repeatable units of five architectures: (i) cubic, (ii) spherical, (iii) X, (iv) diamond, and (v) gyroid; (b) 13-93B3 scaffolds with different architectures after sintering.

The porosities of all the five architectures were designed to be 50, 60, 70, and 80%. However, as mentioned earlier, several factors like laser spot diameter, effectiveness in removing the unsintered powder, and shrinkage of the green part during post-processing affected the porosity of the actual part after sintering. The laser spot diameter of the DTM Sinterstation 2000 used in this study was ~450 μm . The resolution of laser spot would cause heating of the feedstock material on the part bed adjacent to the scanning area of the actual part, effectively reducing the designed pore size in the green part. Although the resolution could be improved with a smaller laser spot, the results mentioned in the current study are based on the laser spot available for the DTM 2000 Sinterstation. The apparent porosities of the sintered scaffolds were measured using Archimedes principle and are presented in Table 2, and the average pore sizes measured using optical microscope are presented in Table 3. The measured porosity results were all ~20% lower when compared to their original designs. Therefore, it has to be noted that along with the shrinkage factor, the difference in porosity factor should also be accounted for while fabricating porous parts using the indirect SLS fabrication process. The measured porosity values were used to plot the graphs in the proceeding sections of the paper.

Table 2. Differences in porosities: designed in CAD vs. measured after sintering.

Architecture	Porosity in %			
	50	60	70	80
Cubic	33.38	39.91	53.88	65.76
Spherical	31.53	42.04	49.02	60.58
X	27.79	34.59	43.17	54.98
Diamond	33.85	39.87	46.73	61.37
Gyroid	34.31	40.91	49.4	59.46

Table 3. Pore sizes of the sintered scaffolds at various porosities (in %).

Architecture	Pore size (μm)			
	50	60	70	80
Cubic	500	700	950	1300
Spherical	500	650	800	900
X	400	550	700	1200
Diamond	800	900	1000	1200
Gyroid	800	900	1000	1100

3.2. Effect of Architecture

Figure 2 shows the difference in the compressive strengths of the scaffolds made with different architectures at measured porosity levels of about ~30% and ~60%. The vertical error bars represent the standard deviation of the measured compressive strength and the horizontal error bars represent the standard deviation in the measured porosity of the scaffolds. The scaffolds with a cubic architecture, and a porosity of ~33%, offered the highest compressive resistance among all of the scaffolds. This can be attributed to the struts in the z-direction which can carry a majority of the load, whereas, such a design feature is not present in any of the other architectures. The spherical and gyroid architectures offered a similar resistance which is followed by the diamond architecture. The scaffolds with the X architecture offered the least

resistance (7.4 MPa at ~28% porosity) compared to diamond architecture (7.2 MPa at ~34% porosity) during the compressive tests as the struts oriented at an angle of 45° to the base plane might not be ideal for compressive loads. Out of the two designs closely mimicking the trabecular bone, the gyroid seems to offer higher resistance than the diamond architecture because of the relatively thick (~1.3 mm for gyroid compared to ~0.9 mm for diamond) and wavy nature of the struts. The compressive strengths of the scaffolds at the lower porosity level (~30%) fall in the range of the higher end of the range of compressive strengths for a human trabecular bone which ranges between 2 and 12 MPa [16], whereas the strengths measured for the scaffolds at higher porosity values (~60%) fall towards the lower range of the strength of human trabecular bone. The effect of different architectures at higher porosities (>60%) can be termed as not significant for load-bearing bone repair applications because of the little difference in compressive strengths of the scaffolds. Also, these higher porosity scaffolds during SBF tests have been shown to have a similar percentage reduction in strength, irrespective of architecture (discussed in detail in Section 3.4). This shows that the internal architecture design parameter could play a key role when fabricating implants at lower porosity levels for load-bearing applications.

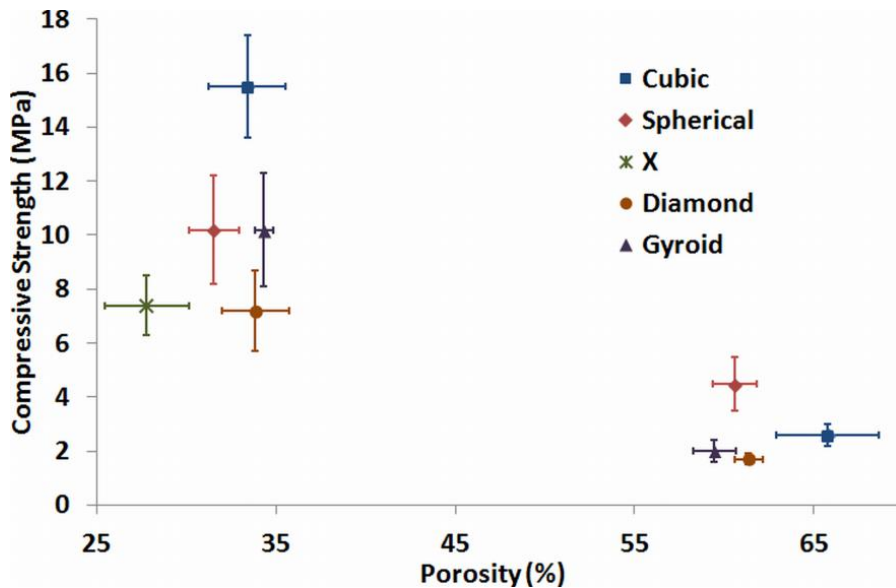


Figure 2. Compressive strengths for 13-93B3 scaffolds fabricated with five different pore geometries and at ~30% and ~60% porosity.

3.3. Effect of Porosity

Figure 3 shows the variation in compressive strengths of the five architectures at different porosities along with an optical image of the sintered scaffolds of diamond architecture at four porosity levels. Although the results show that the scaffold with cubic architecture provides the highest compressive strength at ~33% porosity, and the rate of reduction in strength is higher when compared to the rate of reduction in strength among all the scaffolds with different architectures. The scaffolds with the spherical architecture exhibited the smallest rate of reduction in compressive strength based on the slope of curve. The other three architectures namely, X, diamond, and gyroid have a similar rate of reduction in the compressive strengths

with respect to porosity. The reason for the higher reduction rate for the scaffolds with cubic architecture could be due to the design of the unit cube of this structure. To increase the porosity in the CAD model, the distance between the struts was increased, along with a reduction in the diameter of the strut, which may have resulted in a reduced resistance during compression tests. In the case of scaffolds with the spherical architecture, the absence of struts to carry the load during compression tests results in the least effect on the rate of reduction with respect to increasing the porosity level.

Finite element analysis (FEA) was performed to predict the compressive strengths of the scaffolds with the help of commercially available Abaqus software. For this purpose, the shrinkage and porosity reduction factors were incorporated in the CAD models. The files were modeled with 3D tetrahedral elements with sizes ~ 0.1 mm. The total number of elements for each of the models was kept in the range of 300,000 to 350,000. The ultimate strength of the 13-93B3 material was determined experimentally by fabricating a solid dense cylinder and performing the compressive tests. The density of the solid dense cylinder was considered to have the material's theoretical density (2.164 g/cc) because the same density will be achieved for all the SLS scaffolds as they go through the same heat treatment schedule. A Poisson's ratio of 0.2 was assumed, which is typical for a bioceramic [17]. A 1.2% strain failure criterion was adopted to determine the failure of the specimen, which is typical for a porous bioactive glass specimen. The results in Figure 3 show that FEA can be used to achieve a fairly good estimate of the compressive strengths of the scaffolds fabricated with bioactive glass.

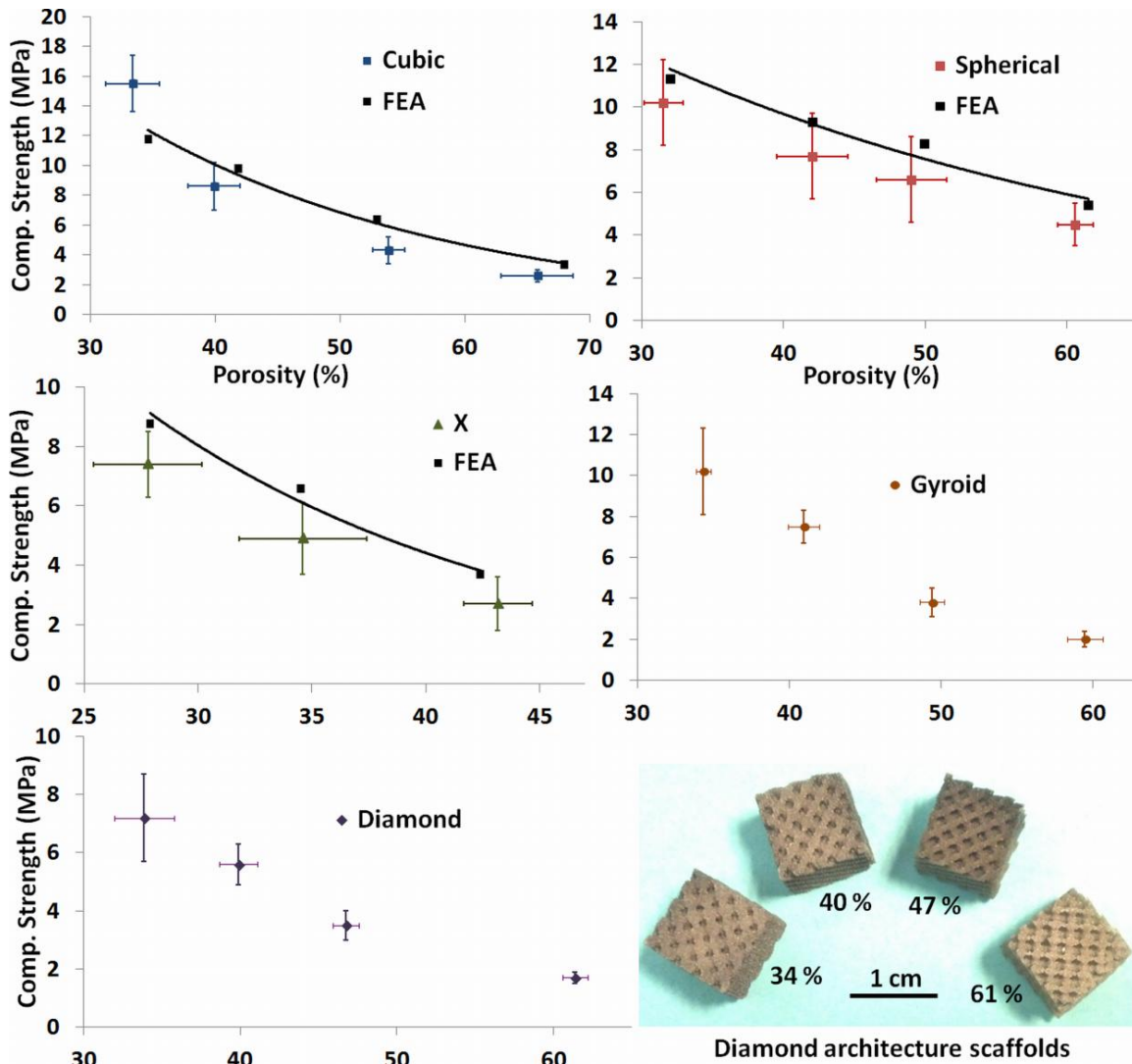


Figure 3. Variation of compressive strength of scaffolds with different architectures at various porosities.

3.4. SBF Tests

The scaffolds were mechanically tested in a wet state after immersion in SBF for one week. The compressive strength for each of the scaffolds was measured to be less than, or about, 2 MPa, which is towards the lower end of the range of compressive strength (2 – 12 MPa) of human trabecular bone [16]. The only exceptions were the scaffolds designed for 50% in CAD (actual measured porosities were ~33% and ~32% as shown in Table 2) with cubic and spherical architectures. The compressive strengths of these scaffolds after one week were measured to be ~4 MPa, which could be due to the relatively thick struts, smaller pores, and higher compressive strengths in their dry state. The reduction in the compressive strengths of the scaffolds with different architectures from ‘as-sintered dry state’ to ‘wet state’ after immersion in SBF for one week is shown in Figure 4. Among the scaffolds which were designed for 80% porosity (actual measured porosities range between ~55% – 65%; see Table 2), irrespective of the architecture, the reduction in compressive strength in the wet scaffolds is more than ~90% when compared to

the as-sintered dry scaffolds. The ~90% reduction in strength could be due to the large pores measuring about ~1 mm in the scaffolds that were designed for 80% porosity (see Table 3). This allows the SBF to contact and react with the inside surface of the scaffold in an efficient manner. Among the scaffolds with lower porosities, the spherical architecture has the lowest reduction in compressive strength (57 – 65%), and the scaffolds with diamond architecture have the highest reduction in compressive strength (80 – 87%). In comparison, the reduction in strength for the scaffolds fabricated using the Robocasting technique was reported to be around ~85% after 30 days [5]. This shows that the percentage reduction in the strengths of the SLS scaffolds is much higher when compared to the Robocasting scaffolds even when the scaffolds are made with the same bioactive glass. This could be because of the surface area that is offered for the scaffolds with complex architectures and also with the increased surface area associated with the SLS process itself (increased surface roughness of the struts) when compared to the Robocasting process (filaments/struts having smoother surface finish). This difference leads to the variable rates of degradation of the scaffolds when immersed in the SBF solution. The SBF results indicate that the SLS process could provide an opportunity, to a certain extent, to control the rate of degradation of scaffolds by selecting an appropriate architecture for the scaffold. For example, the diamond architecture could be the choice for the scaffold fabricated with a silicate bioactive glass, which typically has a slower conversion rate, so as to augment the rate of degradation.

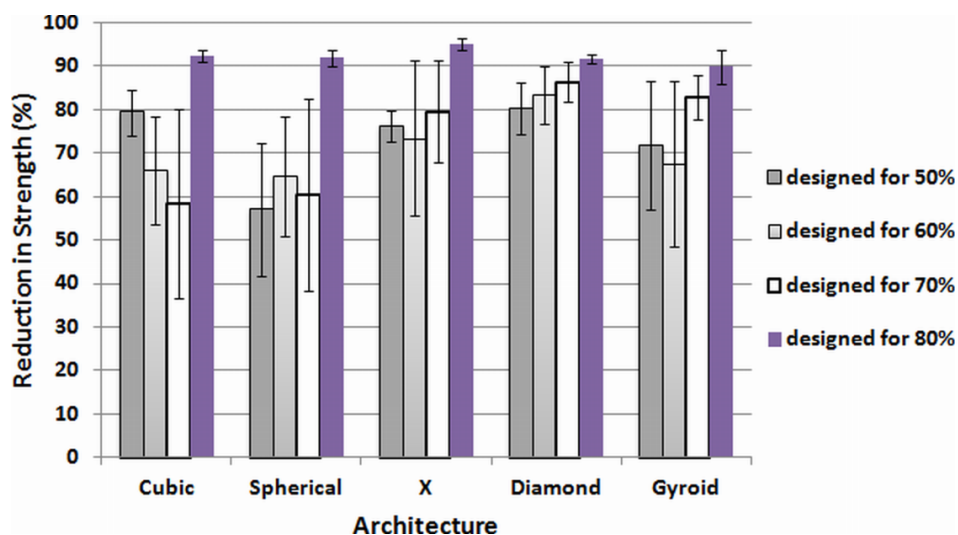


Figure 4. The comparison of reduction in compressive strengths of scaffolds with different architectures and porosities after immersion in SBF for one week.

After testing, the scaffolds were dried at room temperature, sputter coated with gold-palladium, and investigated using SEM. Specifically, SEM was used to look for any crystal like formations on the surface, which were typically formed within one week of the scaffolds' immersion in SBF. Figure 5 shows SEM images of a representative “X” architecture scaffold taken out of the SBF after 7 days. The outer surface morphology of the SLS scaffold is shown in Figure 5(a). Figure 5(b) shows the fracture surface of the scaffold. The reacted surface of the scaffold with SBF can be clearly distinguished with an unconverted 13-93B3 glass core as indicated in the image. A higher magnification image indicating the crystal like formations on the surface of the scaffold after reacting with the SBF is shown in Figure 5(c).

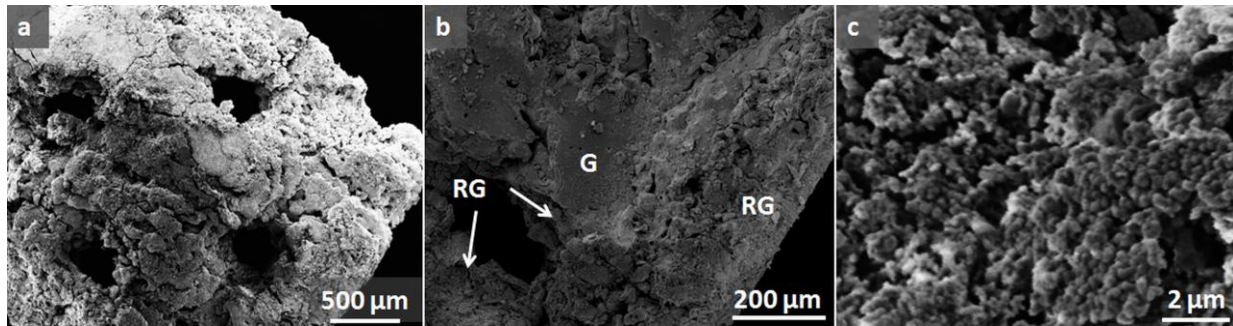


Figure 5. SEM images of a scaffold after immersion in SBF for 7 days: (a) outer surface morphology, (b) fracture surface of the scaffold indicating the reacted glass (RG) on the outer surface and unconverted glass (G), (c) higher magnification image shows crystal-like formations on the surface of the scaffold.

4. Conclusions

It is concluded that among the borate-based bioactive glass scaffolds fabricated by the selective laser sintering (SLS) process, the cubic pore architecture provides the highest compressive strength at lower porosities (< 40%). However, scaffolds with the cubic architecture also exhibit the highest rate of reduction in the compressive strength with increased porosity among all the architectures considered in this study. The effect of different architectures at higher porosities (> 60%) is not significant for load-bearing bone repair applications because of the small variability in the compressive strengths of the scaffolds. The compressive strengths at higher porosity levels (>60%), irrespective of the architecture, fall in the lower range of the compressive strength of a human trabecular bone. The finite element analysis has provided a close estimate of the compressive strengths of the scaffolds fabricated using the SLS process. The simulated body fluid tests indicate that the spherical architecture has the lowest percentage reduction and the diamond architecture has the highest percentage reduction in compressive strengths for scaffolds fabricated at similar porosities. Therefore, the SLS process could provide an opportunity, to a certain extent, to control the rate of degradation of scaffolds by selecting an appropriate architecture for the scaffold.

Acknowledgements

The authors thankfully acknowledge the help of Priyank Madria for assistance and Mo-Sci Corp., Rolla, MO., for kindly supplying the 13-93B3 borate bioactive glass used in this work.

References

- [1] Hench, L.L., Wilson, J., An Introduction to Bioceramics (Singapore: World Scientific Publishing Co. Pte. Ltd.) p 47 (1993).
- [2] Hench, L.L., The story of bioglass. *J Mater Sci: Mater Med.* 17, 967–978 (2006).
- [3] Rahaman, M.N., Day, D.E., Bal, B.S., Fu, Q., Jung, S.B., Bonewald, L.F., Bioactive Glass in Tissue Engineering. *Acta Biomater.* 7, 2355-2373 (2011).

- [4] Fu, Q., Rahaman, M.N., Fu, H., Liu, X., Silicate, borosilicate, and borate bioactive glass scaffolds with controllable degradation rate for bone tissue engineering applications. I. Preparation and in vitro degradation. *J. Biomed. Mater. Res.* 95A 1 164-171 (2010).
- [5] Deliormanli, A., Rahaman, M.N., In vitro evaluation of silicate and borate bioactive glass scaffolds prepared by robocasting of organic based suspensions. *Cer. Eng. Sci. Proc.* 33(6) 11-20 (2012).
- [6] Deliormanli, A., Liu X., Rahaman M.N., Evaluation of borate bioactive glass scaffolds with different pore sizes in a rat subcutaneous implantation model. *J Biomater Appl.* 885328212470013.
- [7] Cai, S., Xi, J., A control approach for pore size distribution in the bone scaffold based on the hexahedral mesh refinement. *Computer-Aided Design.* 40, 1040-1050 (2008).
- [8] Challis, V.J., Roberts, A.P., Grotowski, J.F., Zhang, L-C., Sercombe, T.B., Prototypes for bone implant scaffolds designed via topology optimization and manufactured by solid freeform fabrication. *Advanced Engineering Materials.* 12, 1106-1110 (2010).
- [9] Melchels, F.P.W., Bertoldi, K., Gabbriellini, R., Velders, A.H., Feijen, J., Grijpma, D.W., Mathematically defined tissue engineering scaffold architectures prepared by stereolithography. *Biomaterials.* 32, 2878-2884 (2010).
- [10] Guo, N., Leu, M.C., Additive manufacturing: technology, application and research needs. *Front. Mech. Eng.* (2013).
- [11] Kolan, K.C.R., Leu, M.C., Hilmas, G.E., Velez, M., Selective laser sintering of 13-93 bioactive glass. *Proc. of the 21st Annual Int. Solid Freeform Fabrication Symp. Austin, TX* 504-512 (2010).
- [12] Kolan, K.C.R., Leu, M.C., Hilmas, G.E., Brown, R.F., Velez, M., Fabrication of 13-93 bioactive glass scaffolds for bone tissue engineering using indirect selective laser sintering. *Biofabrication.* 3, 025004 (2011).
- [13] Kolan, K.C.R., Leu, M.C., Hilmas, G.E., Velez, M., Effect of material, process parameters, and simulated body fluids on mechanical properties of 13-93 bioactive glass porous constructs made by selective laser sintering. *Journal of the Mechanical Behavior of Biomedical Materials.* 13, 14-24 (2012).
- [14] Kokubo, T., Takadama, H., How useful is SBF in predicting in vivo bone bioactivity? *Biomaterials.* 27(15) 2907-2915 (2006).
- [15] <http://k3dsurf.sourceforge.net/>
- [16] Carter, D.R., Hayes, W.C., Bone compressive strength: the influence of density and strain rate. *Science.* 194 1174-76 (1976).
- [17] Park, J., *Bioceramics: Properties, Characterizations, and Applications* (New York: Springer Science+Business Media, LLC) p 31 (2008).